DCEA Disaster in Civil Engineering and Architecture

POPULAR SCIENTIST

Research Article

Seismic Performance of IWF and Double-channel Bracings in CBF Systems under Random Variable Amplitude Loading

Arief Panjaitan[a,*], Yulia Hayati[a], Rizki Asmaijar[b], Masaru Shimizu[c]

[a]Department of Civil Engineering, Faculty of Engineering, Universitas Syiah Kuala, Banda Aceh, 23111, Indonesia

[b]Graduate Program of Civil Engineering, Faculty of Engineering, Universitas Syiah Kuala, Banda Aceh, 23111, Indonesia

[c]Civil Engineering Department, Nagoya University, Furo-Cho, Chikusa-Ku, 464-8601, Japan

***Corresponding Author:** Arief Panjaitan (arief_panjaitan@usk.ac.id)

Articles History: **Received:** 29 October 2025; **Revised:** 10 January 2026; **Accepted:** 20 January 2026; **Published:** 3 February 2026

Abstract

The Concentrically Braced Frame System (CBFs) is one of the structural systems that can withstand earthquake loads. In CBFs, the braces are an essential component to dissipate seismic energy. This research aims to find an alternative to enhance seismic capability by comparing two different sections of CBF braces: the IWF section (BU1) and the double-channel sections (BU2). Both sections have equal sectional areas, but the double-channel sections have higher cross-sectional inertia. The two brace models were then loaded by Random Variable Amplitude Loadings (RVAL). The results showed that the BU1 demonstrated better seismic capability in terms of strength, stiffness, and dissipated energy than the BU2. Moreover, to determine the effect of amplitude variability on the performance of the Single IWF and Double-channel bracing, the influence of the RVAL was analyzed, and it was revealed that increasing and decreasing displacement amplitude tend to cause increasing and decreasing strength in a polynomial trend. Meanwhile, escalating and reducing displacement amplitude leads to increasing and decreasing strength in the power trend.

Keywords: CBF Systems, Bracing Performance, Random Variable Amplitude Loading, Seismic Capability, Dissipated Energy

Introduction

Indonesia, located in Southeast Asia, has geographical characteristics that make it vulnerable to earthquakes. The Concentric Bracing Frame System (CBF) is a suitable configuration because it has good stiffness, which can improve the structure's performance against lateral loads due to earthquakes by increasing the stability and stiffness of the structure [1-5].

In CBF, brace is essential component that plays important role in dissipating energy from the earthquake, so that several modifications have been conducted

in brace to enhance its performance in former studies, i.e., by utilizing Shape Memory Alloy (SMA) with the Super Elastic characteristics and high damping as the braces material; investigating the seismic performance of single bracing, double-section bracing with batten plates, double-section bracing with lacing; and conducting comparative study of the implementation initial bracing (without replacing old braces) and CBFs with new bracing that replaces previous bracing at the CBF tested under earthquake load [6-13].

The influence of bracing configuration in CBFs, i.e., X, V, inverted V, and two-story X and combination of two systems, i.e., Self-Centering Braces (SCBs) and Buckling-Restrained Braces (BRBs) were evaluated to the earthquake load at the past studies, where the research work revealed that the brace configurations determined the dimensions of the CBFs' components and the structure can obtain the advantages from SCBs-BRBs combination [14-17]. Observations on fracture and low-cycle fatigue of the CBF brace in Seismic Self-Centering Concentrically Braced Frame (SC-CBF) under repeated loads have also been carried out at previous research works [18-19]. Former works also conducted nonlinear dynamic and pushover analysis for multi-storey CBFs for different seismic intensities [20-22]. Another researcher analyzed the CBFs referring to the SNI-1729-2020 and AISC 341-16 [23].

This study evaluated the seismic performance of two different section bracings, i.e., double-channels and IWF-section bracings. Both bracings were modelled in Abaqus v6.14 and loaded with Random Variable Amplitude Loading (RVAL). The observation was conducted on the seismic performances of bracings, i.e., strength, stiffness, and dissipated energy. Eventually, the effectiveness of involving double-channel bracings was investigated.

Research Methodology

Bracing Models

The object studied is the bracing element modelled in Abaqus v6.14. The materials used as the bracing element model in this study are the IWF100.100.6.8 profile and the 2C.100.50.5.7.5 double-channel with a coupling plate (6 mm thick) as the connector. In this study, the Single IWF and Double-channel specimens will be subjected to Loading Histories 1 and 2, and their performance will then be compared to determine which configuration exhibits better performance.

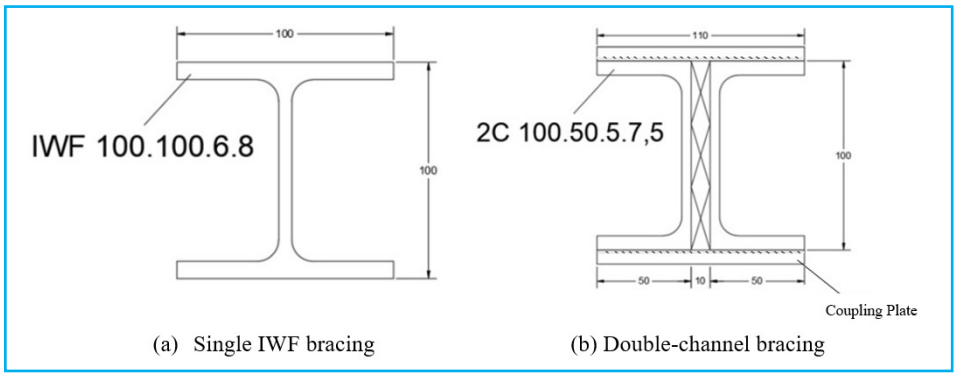

Figure 1. Bracing models (unit: mm)

The Single IWF and Double-channel bracing specimens share identical geometric properties in terms of length, height, and cross-sectional area. The profile length is 4000 mm, the section height is 100 mm, and the cross-sectional area is 100 mm^2. For the Double-channel configuration, the spacing between the two profiles is 10 mm. The cross-sectional configurations of the bracing models are presented in Figure 1 and summarized in Table 1.

Table 1. Bracing models characteristics

No	Bracing notation	Sectional area	Loading history
1	BU11	Single IWF	RVAL 1
2	BU12	Single IWF	RVAL 1
3	BU21	Double-channels	RVAL 2
4	BU22	Double-channels	RVAL 2

Data Types And Sources

The primary data used in this study are loading history data and hysteretic curves. The random variable amplitude loading history (RVAL) is arranged randomly to represent the actual earthquake loading conditions by the principle of cyclic loading history in structural engineering. Earthquake loads are generally irregular and consist of dynamically changing tensile-compressive cycles [13]. In the separate research work, the previous study [13] used the Two-Step Variable Amplitude (TSVA) approach, where tensile and compressive displacements have the same value. However, in this study, the magnitude of tensile and compressive displacements is different because it adjusts the characteristics of the RVAL, which describes the variation of earthquake loads more randomly and complexly. Two RVALs are applied in this study, as illustrated in Figures 2 and 3.

The hysteretic curve is obtained from a loading simulation with the utilization of Abaqus v16.4 software. The bracing test specimen is modeled in Abaqus v6.14, and then the RVAL loading simulation is performed on the test specimen model. A hysteretic curve will be generated from the RVAL loading simulation on this test specimen, describing the relationship between load and displacement, to compare the bracing strength.

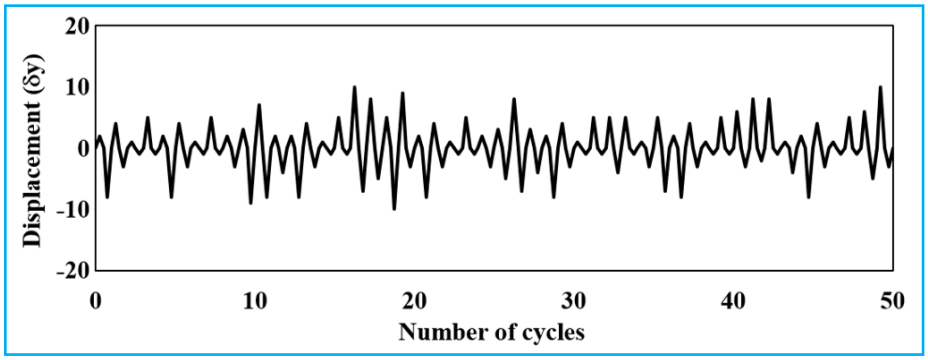

Figure 2. RVAL 1 (-10 δy ≤ δ ≤ 10 δy)

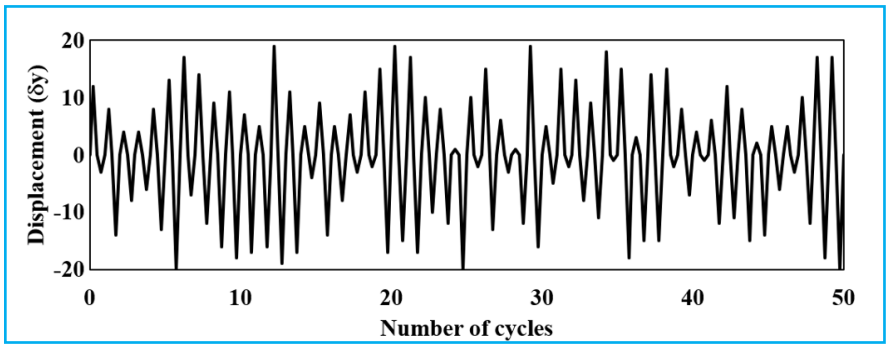

Figure 3. RVAL 2 (-20 δy ≤ δ ≤ 20 δy)

The secondary data used in this study are data on the mechanical properties of steel and yield transfer. The mechanical properties of steel are the characteristics of steel related to the response of steel to the force or load given, namely the yield and ultimate stress and its strain. This study used the stress and strain obtained based on tests conducted in previous studies [13].

Yield displacement is the deformation that occurs in steel material when the stress reaches the yield point, which is the point where the capacity curve changes from a linear condition to a parabolic condition. Yield displacement can be obtained by tensile testing to produce a tensile capacity curve of the load-displacement relationship. In this study, a yield displacement of 4.3 mm was used. The yield displacement will later be multiplied by the amplitude coefficient in RVAL because the cyclic load simulation is based on large displacements such as those found in earthquake loads.

Modelling and Loading Process

In the initial stage, the bracing is modeled with a 3D hexahedral element with eight nodes. Each node has six DOFs consisting of 3 DOFs in the translation direction (u, v, w) and 3 DOFs in the rotation direction (φx, φy, φz). On the bottom side of the bracing, a clamp is provided so that there is no deformation in the bracing in the translation direction, and the top side is provided with a roller placement where displacement in the direction parallel to the bracing is allowed to be given.

On the top side of the bracing, a Reference Point (RP) element is added as a reference point for applying tensile loads. RP is placed at the center of gravity position of the cross-section to ensure that the cyclic load given will work concentrically. To bind the top side of the bracing cross-section to the RP, a rigid body constraint (RC) is used as a feature available in Abaqus v6.14, as shown in Figure 4.

Cyclic loading is done on RP, and due to the presence of RC on the upper side, the brace will experience tensile and compressive forces. The provision of tensile deformation provides tensile force on the model until it reaches the deformation point on RVAL, which is continued with compressive deformation, which provides compressive force until it reaches the planned deformation on RVAL. The provision of displacement control values that follow RVAL will produce a hysteretic curve in the load-displacement relationship.

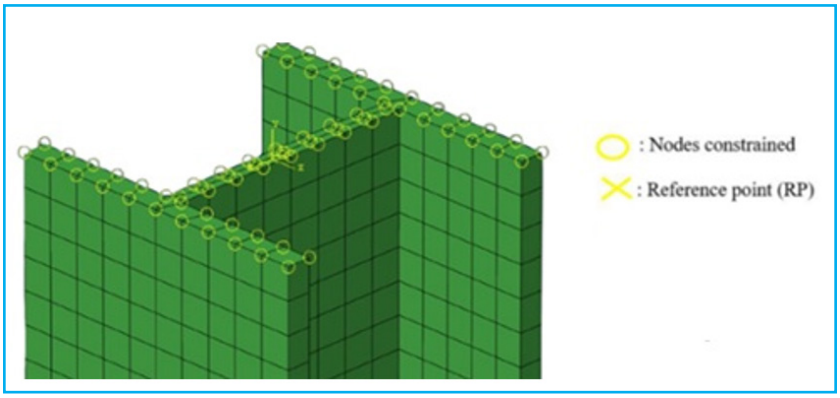

Figure 4. RP bonding with the bracing models

The characteristics of CBF bracings are provided in Figures 5 and 6. In Figure 5(a), the Single IWF bracing model is presented in transverse view, and in Figure 5(b), the transverse view of the double-channel bracing model is depicted. In Figure 6(a), the model of the single IWF bracing is provided in longitudinal view, and the model of the double-channel bracing in longitudinal view is illustrated in Figure 6(b).

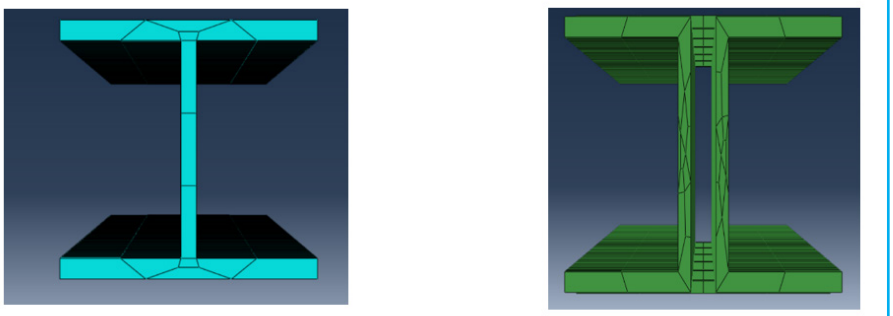

Figure 5. Transverse views of bracing models

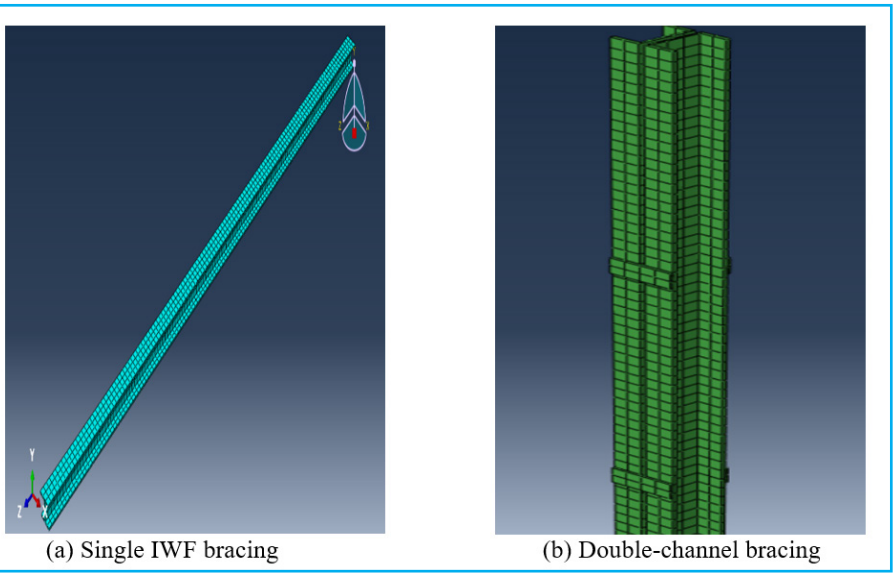

Figure 6. Longitudinal views of bracing models

Results And Discussion

Initial analysis of the bracing performance was carried out by obtaining a hysteretic curve through cyclic loading simulation based on the RVAL loading pattern. The simulation results are in the form of a hysteretic curve that shows the relationship between load and displacement. Hysteretic curves are generated from the simulation of the two bracing models in Figure 7. Figures 7(a) and 7(b) show that the double-channel bracing shows a better hysteretic curve by showing a larger and more stable hysteretic loop. This is because the double-channel has greater inertia, and the distance and coupling plate connecting the double-channel also have a significant influence, so that it can withstand tensile and compressive loads better than the Single IWF bracing.

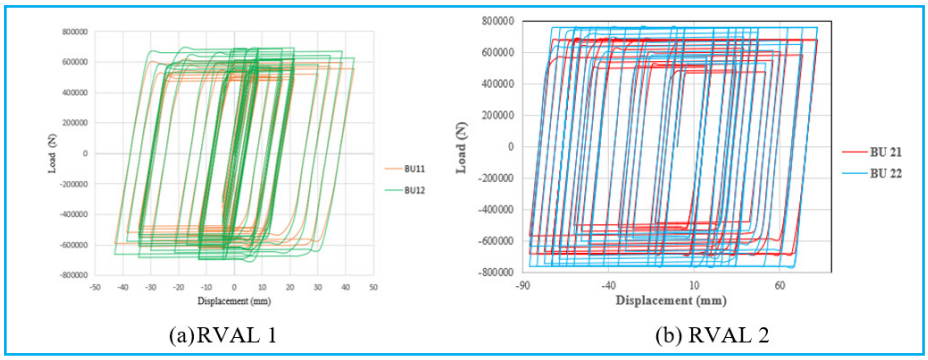

Figure 7. Hysteretic curves of the single IWF and double-channel bracing

Tensile and compressive strengths are obtained from the maximum force at each peak of the hysteretic curve. In one cycle, the hysteretic curve contains maximum tensile and compressive forces. The maximum tensile and compressive forces are the tensile and compressive strengths of the braces. Based on the hysteretic curve obtained, the graph in the following Figure shows the tensile and compressive strengths.

The graph of the relationship between strength and displacement is shown in Figures 8 and 9. The figures show that it has the same pattern but with different values. Under the RVAL 1, Figure 8(a) presents the tensile strength of BU 11 and BU 12 are 619429 N and 694092 N. In Figure 8(b), the compressive strength values are 620654 N and 696859 N. When they are compared to the IWF profile, the strength of the double-channel profile is higher by 12.5 %

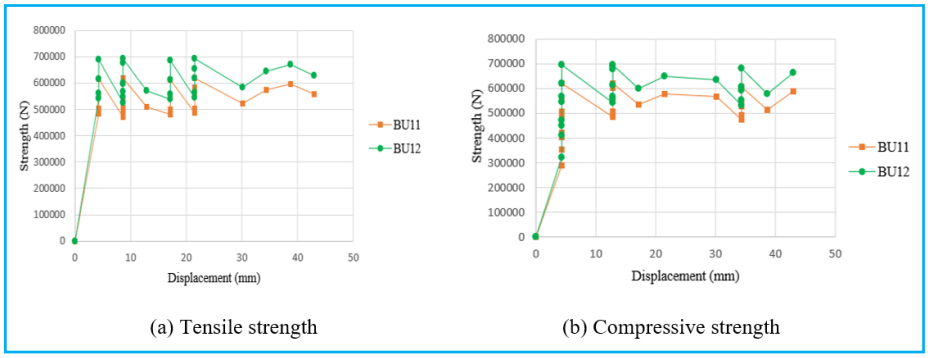

Figure 8. Tensile and compressive strengths of both bracing models with RVAL 1

Under the RVAL 2, as shown in Figure 9(a), the tensile strengths of BU 21 and BU 22 are 681699 N and 761402 N. In Figure 9(b), the compressive strength values are 681699 N and 761402 N. When they are confirmed to the IWF profile, the strength of the channel profile has increased on average by 11.67%.

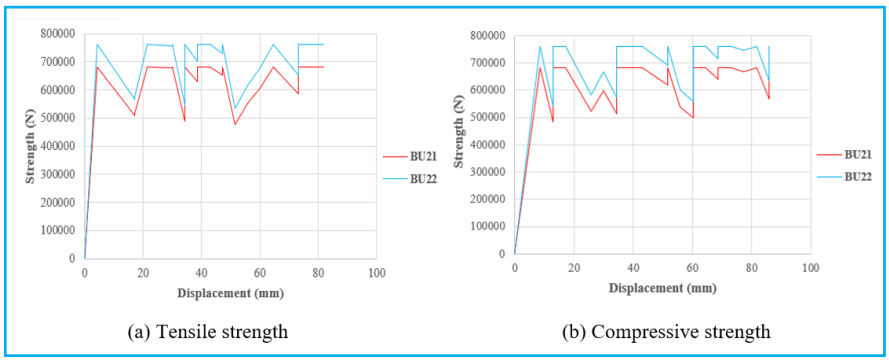

Figure 9. Tensile and compressive strengths of both bracing models with RVAL 2

After obtaining the strength value, the stiffness parameter can be calculated by dividing the load value by the displacement. In this case, the load in question is the maximum load (strength), while the displacement used is the displacement when the peak load occurs. Based on data from the hysteretic curve, the stiffness values for the tensile and compressive directions are obtained, as shown below.

The relationships between stiffness and displacement on bracing models are shown in Figures 10 and 11. There are similar patterns but with different values. In Figure 10(a), the maximum tensile stiffnesses of bracing models BU 11 and BU 12 with RVAL 1 are 143132.79 N/mm and 160703.49 N/mm. Meanwhile, in Figure 10(b), the maximum compressive stiffness is 144030.93 N/mm (BU 11) and 161717.67 N/mm (BU 12), respectively.

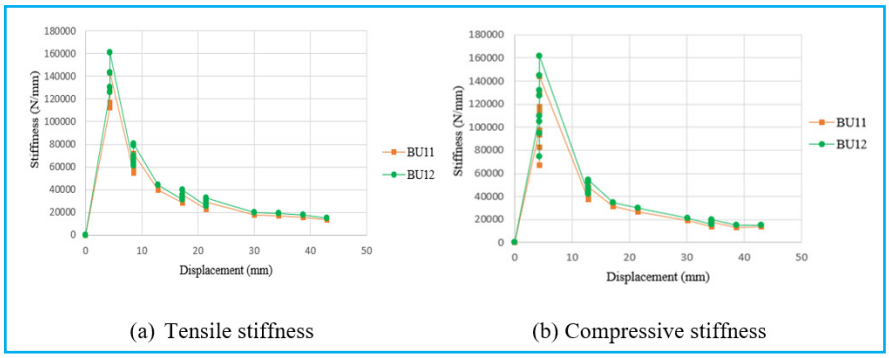

Figure 10. Tensile and compressive stiffness of both test specimens with RVAL 1

From the graph, it can be seen that the channel profile has a greater stiffness than the IWF profile stiffness. On average, the stiffness of BU 12 is about 12.08% greater than BU 11. In addition, the graph shows that stiffness decreases with increasing displacement. For example, in BU 11, the stiffness was recorded at 18811.96 N/mm when the displacement was 30.1 mm and decreased to 13839.56 N/mm when the displacement reached 34.4 mm. This decrease was due to repeated loading. The maximum tensile stiffness in Figure 11(a) of BU 21 and

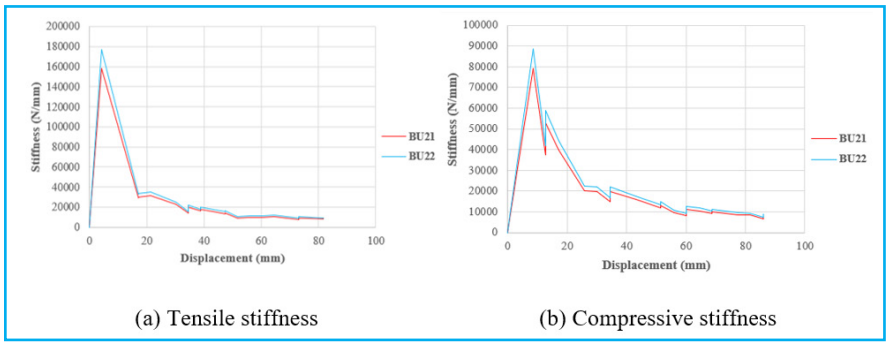

Figure 11. Tensile and compressive stiffness of both test specimens with RVAL 2

BU 22 test specimens with RVAL 2 was 158533.95 N/mm and 177069.77 N/mm. Meanwhile, in Figure 11(b), the maximum compressive stiffness was 79266.98 N/mm (BU 21) and 88534.88 N/mm (BU 22), respectively. From the graph, it can be seen that the channel profile is stiffer than the IWF profile. On average, the stiffness of BU 22 is about 11.67% greater than that of BU 21.

Dissipated energy is the ability of a structure to absorb and release energy. Dissipated energy is calculated for each half cycle because, in one cycle, there is a displacement in the tensile and compressive directions whose values are not always the same. The area of the hysteretic curve in each half cycle is used as the basis for calculating dissipated energy.

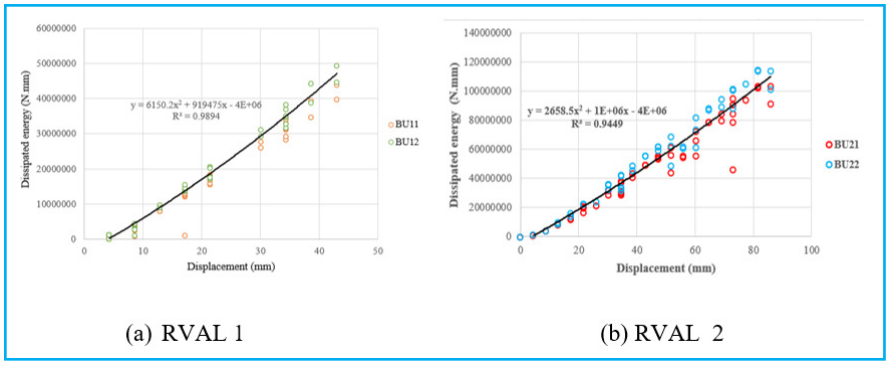

Figure 12. Dissipated energy

Figure 12(a) shows a comparison graph of the dissipated energy of RVAL 1, and Figure 12(b) shows a comparison of the dissipated energy of RVAL 2. From both graphs, it can be seen that the channel profile has a better dissipated energy value compared to the IWF profile. The maximum value of dissipated energy of each bracing model is 43825.42 Nmm for BU 11, 49173.48 Nmm for BU 12, 103705.21 Nmm for BU 21, and 114624.60 Nmm for BU 22. Compared to the IWF profile, the dissipated energy of the channel profile increases by an average percentage of 2.35% in RVAL 1 and 5.26% in RVAL 2.

Conclusion

Several conclusions can be drawn from the evaluation results of the Single IWF and Double-channel CBF bracing models tested under the RVALs. The study showed that the Double-channel bracing section performs better than

the Single IWF profile in terms of strength, stiffness, and dissipated energy. Furthermore, related to the amplitude alteration in RVAL, it was found that when the displacement amplitudes were decreased, the strength decreased with a polynomial trend, the stiffness increased with a power trend, and the dissipated energy decreased with a polynomial trend. On the contrary, as the displacement amplitude increased, the strength increased in a polynomial trend, and the stiffness decreased in a power manner. Eventually, it was recommended to implement the Double-channel bracing in CBF to enhance the seismic capabilities of the buildings, particularly when they are located in seismic hazard areas.

Acknowledgement

The authors appreciate the individuals who were involved in the data collection process, and specially, the Department of Civil Engineering of Universitas Syiah Kuala.

Conflicts of Interest

All authors declare that they have no conflict of interests.

Author Contributions

Arief Panjaitan: writing- reviewing and editing, methodology, investigation, supervision. **Yulia Hayati:** conceptualization, project administration, writing-reviewing and editing, supervision. **Rizki Asmaijar:** writing-original draft, formal analysis, visualization. **Masaru Shimizu:** conceptualization, supervision.

Data Availability Statement

The data used to support the findings of this study are included within the article.

References

[1] S. Alhikmi, Analisis Struktur Beban Gempa Dinamik 8,5 SR pada Bangunan Rumah Tinggal 3 Lantai Slawi Kab. Tegal Berdasarkan Perhitungan SAP2000, Skripsi Sarjana, Fakultas Teknik dan Ilmu Komputer, Universitas Pancasakti, Tegal, 2024.

[2] A. A. Bahri, Kinerja Bresing Diagonal SRBK Berpenampang Tunggal dan Ganda terhadap Riwayat Pembebanan Two-Step Variable Amplitude, Skripsi Sarjana, Program Studi Sarjana Teknik Sipil, Universitas Syiah Kuala, Banda Aceh, 2024.

[3] K. C. Cari and D. T. A. Bramantoro, “Pengaruh Bentuk Bracing Eksentris pada Struktur dengan Analisis Gempa Respon Spektrum,” Composite: J. Civil Eng., vol. 2, no. 1, pp. 25–32, 2023, doi: http://dx.doi.org/10.26905/jtsc.v2i1.10050

[4] A. K. Chopra, Dynamics of Structures: Theory and Applications to Earthquake Engineering, 4th ed., London: Pearson, 2017.

[5] C. Thongchom, A. Bahrami, A. Ghamari, and O. Benjeddou, “Performance improvement of innovative shear damper using diagonal stiffeners for Concentrically Braced Frame Systems,” Buildings, vol. 12, pp. 1–17, 2022, doi: http://dx.doi.org/10.3390/buildings12111794

[6] A. M. Emilidardi, Analisis Beban Statik Model Numerik Finned Tabular Shear Panel Damper Multiarah secara Metode Elemen Hingga, Skripsi Sarjana, Departemen Teknik Sipil dan Lingkungan, Universitas Gadjah Mada, Yogyakarta, 2021.

[7] A. Garg and A. Sharma, “Seismic Performance Evaluation of a Multi-Storey Building with Different Braced Frames,” ELK Asia Pacific J. Civil Eng. Struct. Dev., vol. 6, no. 1, pp. 1–17, 2020.

[8] C. K. Halim, L. S. B. Wibowo, M. S. D. Cahyono, and N. Ray, “Studi Pengaruh Variasi Tipe Pengaku Diagonal pada Struktur Bangunan Baja Bertingkat terhadap Perpindahan Lateral,” Narotama J. Tek. Sipil, vol. 4, no. 1, pp. 21–29, 2020.

[9] A. Imran, E. Priskasari, and A. Santosa, “Analisa Perbandingan Gable Frame Baja WF dan Struktur Rangka Baja Siku dan T,” J. Sondir, vol. 1, pp. 7–13, 2017.

[10] V. Mohsenazdeh and L. Wiebe, “Experimental Investigation of a Concentrically Braced Frame with Replaceable Brace Modules,” J. Struct. Eng., vol. 146, no. 11, 2020, doi: http://dx.doi.org/10.1061/(ASCE)ST.1943-541X.0002817

[11] E. Xiong, K. Zu, and Q. Zhang, “Seismic performance analysis of self-centering concentrically braced steel frame structures,” Shock and Vibration, vol. 2020, 2020, doi: http://dx.doi.org/10.1155/2020/8826272

[12] R. Sabelli, C. W. Roeder, and J. F. Hajjar, Seismic Design of Steel Special Concentrically Braced Frame Systems: A Guide for Practicing Engineers, U.S. Dept. of Commerce, 2013.

[13] A. Panjaitan, P. Hasibuan, and M. Haiqal, “Kajian kinerja struktural elemen bresing SRBK dengan tipe penampang tunggal dan ganda terhadap beban siklik,” J. Arsip Rekayasa Sipil Perencanaan, vol. 5, no. 4, pp. 257–264, 2022, doi: http://dx.doi.org/ 10.24815/jarsp.v5i4.2827

[14] T. Y. Yang, H. Sheikh, and L. Tobber, “Influence of the brace configurations on the seismic performance of steel concentrically braced frames,” Front. Built Environ., vol. 5, pp. 1–13, 2019, doi: http://dx.doi.org/10.3389/fbuil.2019.00027

[15] R. Chen, C. Qiu, and D. Hao, “Seismic response analysis of multi-story steel frames using BRB and SCB hybrid bracing system,” Appl. Sci. (Switzerland), vol. 10, no. 1, 2020, doi: http://dx.doi.org/10.3390/app10010284

[16] M. Naghavi, R. Rahnavard, R. J. Thomas, and M. Malekinejad, “Numerical evaluation of the hysteretic behavior of concentrically braced frames and buckling restrained brace frame systems,” J. Build. Eng., vol. 22, pp. 415–428, 2019, doi: http://dx.doi.org/10.1016/j.jobe.2018.12.023

[17] T. Y. Yang, H. Sheikh, and L. Tobber, “Influence of the brace configurations on the seismic performance of steel concentrically braced frames,” Front. Built Environ., vol. 5, 2019, doi: http://dx.doi.org/10.3389/fbuil.2019.00027

[18] A. D. Sen, C. W. Roeder, D. E. Lehman, and J. W. Berman, “Nonlinear modeling of concentrically braced frames,” J. Constr. Steel Res., vol. 157, pp. 103–120, 2019, doi: http://dx.doi.org/10.1016/j.jcsr.2019.02.007

[19] S. Babaei and P. Zarfam, “Optimization of shape memory alloy braces for concentrically braced steel braced frames,” Open Eng., vol. 9, no. 1, pp. 697–708, 2020, doi: http://dx.doi.org/10.1515/eng-2019-0084

[20] Y. W. Li, G. Q. Li, F. F. Sun, and J. Jiang, “Mitigating inter-story drift concentration of concentrically braced steel frames using energy-dissipative columns,” J. Earthq. Eng., vol. 26, no. 1, pp. 221–239, 2022, doi: http://dx.doi.org/10.1080/13632469.2019.1682088

[21] S. Costanzo, M. D’Aniello, and R. Landolfo, “Nonlinear static response of low-moderate ductile chevron concentrically braced frames designed according to Eurocode 8,” Buildings, vol. 13, no. 1, 2023, doi: http://dx.doi.org/10.3390/buildings13010120

[22] S. Sumaidi, W. Kartini, and A. Rumintang, “Analisa perbandingan struktur baja 3 lantai menggunakan sistem CBF dan EBF dengan metode Push Over Analysis,” J. Envirotek, vol. 12, no. 2, pp. 75–81, 2020, doi: http://dx.doi.org/10.33005/envirotek.v13i1.112

[23] J. Aloysius, J. A. Sumito, D. Prayogo, and H. Santoso, “Optimization of concentrically braced steel frame structures based on SNI 1726:2019, SNI 1727:2020, SNI 1729:2020, and AISC 341-16,” in IOP Conf. Ser.: Earth Environ. Sci., IOP Publishing Ltd., 2021, doi: http://dx.doi.org/10.1088/1755-1315/907/1/012010